McMaster University

Advanced Optimization Laboratory

Title:

Optimizing the gVERSE RF Pulse Design via Optimal Control

Authors:

Christopher K. Anand, Stephen J. Stoyan and Tamás Terlaky

AdvOl-Report No. 2005/6

May 2005, Hamilton, Ontario, Canada

Optimizing the gVERSE RF Pulse Design via Optimal Control

Christopher K. Anand, Stephen J. Stoyan, Tamás Terlaky

***Abstract*— Magnetic Resonance Imaging (MRI) is an advanced tomographic technique that is able to produce high resolution cross-sectional images of an object or specimen by exploiting Radio Frequency (RF) pulses. A Variable Rate Selective Excitation (VERSE) pulse is a type of RF pulse that reduces the Specific Absorption Rate (SAR) of molecules in a specimen; SAR leads to an increase in patient temperature during MRI procedures. We develop a selective VERSE pulse that is designed to minimize SAR while preserving its duration and slice profile, called the generalized VERSE (gVERSE), because it allows more general variations of the slice gradient waveform. After the formulation of a rigorous mathematical model that is aimed at minimizing SAR RF levels, the nonlinear gVERSE problem is subsequently solved as an optimal control problem. Using state of the art Sparse Optimal Control Software (SOCS), two separate variations of SAR reducing gVERSE pulses were generated. The Magnetic Resonance (MR) signals produced by numerical simulations were then tested and analyzed by an MRI simulator. Computational experiments involved with the gVERSE model provided surprising constant RF pulse levels and had encouraging results with respect to MR signals. The testing results produced by the gVERSE pulse illustrate the potential advanced optimization techniques have in designing RF pulses, which has already influenced further research in the area.**

I. Introduction to the Problem

Magnetic Resonance Imaging (MRI) produces high resolution cross-sectional images by utilizing selective Radio Frequency (RF) pluses and field gradients. Selective excitations are obtained by applying simultaneous gradient waveforms and an RF pulse with the appropriate bandwidth [13]. Many conventional RF pulse sequences are geared towards generating high definition images, but fail to consider the SAR (Specific Absorption Rate) level of the signal. High levels of SAR during MRI procedures can cause undesired side effects, such as skin burns. Currently, there has been no significant attempt to solve such a dynamical design problem that integrates SAR levels in the highly nonlinear relationship between the RF-gradient pulse pair envelope and its resultant magnetization distribution. Many methods for solving the RF pulse design problem are derived from approximations of the Bloch equation. In our approach, we integrate the Bloch equation in a rigorous nonlinear model that optimizes RF SAR levels, while upholding MRI image resolution.

Several researchers have studied the selective RF excitation problem and employed different optimization methods in their designs. Simulated annealing [17], evolutionary algorithms [20], quadratic optimization [9] and optimal control techniques [8], [19] are the most common. Although they produce solutions that relate to their desired profile, they are computationally intensive and in many cases, their mathematical foundation for the pulse-envelope consisted of relaxed conditions and formulations. Under the optimal control approach in [19], the excitation design leads to an ill-conditioned algebraic problem, which stems from the models attempt to include the Bloch equation in the Chebyshev domain. In [9], Conolly *et al.* design the Variable Rate Selective Excitation (VERSE) pulse that is aimed at reducing MRI SAR levels, however, the model fails to incorporate the complex nonlinear demands of RF pulse sequences.

The problem still remains, as pointed out in [8], [9], there is no sufficient mathematical formulation for pulse-envelope design and one that incorporates SAR reduction in the pulse model. This paper provides both a comprehensive mathematical basis for pulse design, as well as, a dynamical algorithm that includes SAR reduction in an innovative nonlinear optimization model. Using Conolly's *et al.* idea, we design the generalized VERSE (gVERSE) pulse that minimizes the level of SAR during MRI procedures while maintaining strong MR signal quality. The gVERSE pulse is a highly selective pulse that differs from its originator with respect to how SAR is minimized. The letter "g" was added to VERSE because our objective function directly encompasses the high demands of RF pulse levels by allowing the gradient waveform to freely vary, in addition to significantly increasing the dynamics, constraints and degrees of freedom involved in the problem. For the first time in MRI history, we are able to use cutting edge optimization technology to adhere to the demands of RF pulse sequences. By carefully formulating the mathematics behind RF pulse and gradient waveform designs, we develop two separate pulse sequences of which include variable slice gradients, listed as future work in [19]. Both gVERSE sequences show to have great potential in the realm of MR research.

In this paper, we begin with a review of general RF pulse sequences that leads to the development of our new SAR reducing gVERSE pulse model. In Section III, the gVERSE model is fully detailed and the accompanying Nonlinear Optimization (NLO) problem is formulated. The implementation issues involved in computing the gVERSE pulse are described in Section IV. The ideas behind the initial solution and the functionality of the optimal control software used for solving the problem is also mentioned. In Section V, the computational results for the gVERSE pulse are shown for two different test cases. The results are graphically illustrated and then tested by an MRI simulation, where they

Manuscript received May 04, 2005. This work was supported by NSERC Discovery grants, the CRC program, and MITACS.

are analyzed and examined with respect to the MR signals they generate. Our results and MRI simulations clearly show that mathematical optimization can have a strong effect on improving RF pulse sequences.

II. MRI Background

To understand the implications and effects of the gVERSE pulse in MRI we will begin with a short outline of our notation and a review of two different types of RF pulse sequences. For more information with regards to the MR formulations and/or general RF pulses, one can refer to [6], [14], [15].

To begin, we define magnetization as the aggregate magnetic moment of nuclei in a given unit volume. An intrinsic property of atoms with odd atomic weights and/or odd atomic numbers that enables MRI, independently described by Bloch and Purcell in 1946 [6]. Consider a sufficient volume of protons or nuclei, known as a voxel. The rate of magnetization $d\overrightarrow{M}(t)/dt$ is described in the Bloch equation

$$\frac{d\overrightarrow{M}(t)}{dt} = \gamma\overrightarrow{M}(t) \times \overrightarrow{B}(t) + \frac{1}{\tau_1}(M_0 - M_z(t))\widehat{z} - \frac{1}{\tau_2}\overrightarrow{M}_{\perp}(t),$$

where t is time, $\overrightarrow{B}(t)$ is the external magnetic field in the z-axis direction, γ is the gyromagnetic constant, and

$$\overrightarrow{M}(t) = \begin{bmatrix} M_x(t) \\ M_y(t) \\ M_z(t) \end{bmatrix}, \qquad \overrightarrow{M}_{\perp}(t) = \begin{bmatrix} M_x(t) \\ M_y(t) \\ 0 \end{bmatrix}$$

are respectively the net and transverse magnetization vectors. Furthermore, $\widehat{z}$ is the z-axis unit vector, M_0 is the initial magnetization in the $\widehat{z}$ direction, τ_1 is the spin-lattice interaction parameter and τ_2 is the spin-spin interaction parameter. In addition, since a final MR image is produced by controlling and manipulating the external magnetic field, we introduce the vector coordinates $b_x(t),\ b_y(t)$ and $b_z(t)$ to the external magnetic field

$$\overrightarrow{B}(t) = \begin{bmatrix} b_x(t) \\ b_y(t) \\ b_z(t) \end{bmatrix},$$

which will be used in the formulation of the gVERSE pulse.

A. Generic RF pulse

When processing an image, a number of precise RF pulses are applied in combination with synchronized gradients in different dimensional directions. An oversimplification of the MRI procedure would be as follows: First, a specimen or object is positioned in a large main magnet, which creates a uniform magnetic field in one axial direction, known as B_0. Next, an RF coil produces an "RF pulse," which causes the magnetic moments to tip into an orthogonal direction of B_0, called the transverse plane [14]. The RF pulse is only aimed at a specific portion of the object or specimen that the user intends to image. When the magnetic moments tip into the transverse plane they generate a signal that is picked up by receiver coils, which can also be a part of the RF coil. In addition, the RF pulse is accompanied by a gradient waveform

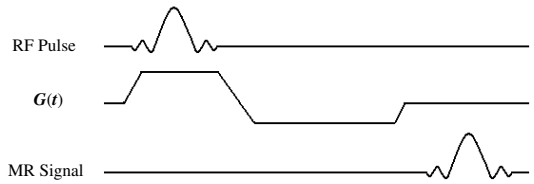

Fig. 1. A generic NMR slice select pulse imaging sequence.

that is used to spatially modulate the signals orientation [6]. Finally, the data information generated by the signal is computationally formulated into a final image. The key ingredient to the formation of any MR image is the unique RF pulse and the accompanying gradient waveform used during the process. There are many different techniques in which RF and gradient waveforms can generate useable signals. Gaussian, Sinc and Echo pulses are a few of the many RF pulse sequences used today. Figure 1 is an illustration of a slice select sinc pulse [14]. Sinc pulses are one of the first types of RF pulses to be used in MRI, which lead to the development of other highly complicated pulse sequences. The Sinc pulse was successful at exciting particular voxels into the transverse plane that would generate signal readings, however, it failed to take into account side effects such as SAR levels. The heating effect experienced by patients during MRI procedures is measured by the level of SAR, which is a direct result of the RF pulse used. The level of SAR becomes particularly important with pediatric patients and as a result the FDA has strict limitations on SAR; which subsequently restricts RF pulse potential and other elements involved in MRI procedures. In addition, as MRI researchers are constantly developing faster scanners, higher Tesla magnets, enhanced software components and improved RF coils, they are all still limited by SAR levels. Hence, RF pulses that consider such a factor are in high demand.

B. The VERSE Pulse

Originally proposed by Conolly *et al.* [9], VERSE pluses were designed to generate MR signals similar to generic RF pulses, however, low pulse SAR levels were incorporated into the model. As mentioned, the SAR of a selective RF pulse is a critical parameter in clinical settings and may limit the use of a particular pulse sequence if the SAR limit exceeds given FDA requirements [15]. Due to the high SAR levels of various RF pluses the scan time for given pulse sequences are restricted [9]. The key innovation with VERSE pulses is to allow a "trade off" between time and amplitude. By lowering RF pulse amplitude the duration of the pulse may be extended [9]. As illustrated in Figure 2, VERSE pulses are similar to generic pulses, however, they contain a flattened center peak and their gradient waveform posses two additional steps. It is this uniform redistribution of the pulse area that allows the decrease in SAR. Conolly *et al.* designed three different types of SAR reducing pulses, each that had constraints on the strength of the RF pulse, however, they differed with respect

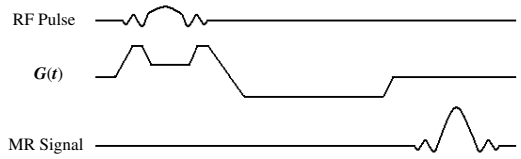

Fig. 2. The VERSE pulse imaging sequence.

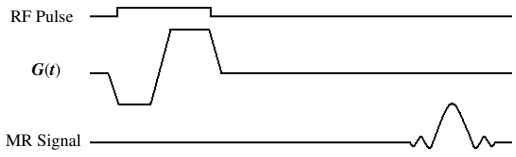

Fig. 3. The gVERSE pulse imaging sequence.

to how they minimized SAR levels. The first model offers the minimum–SAR facsimile pulse for a specified duration, whereby the gradient waveform and RF pulse is integrated in the objective subject to maximum gradient and constant duration constraints. The second, the minimum time formulation, searches for the briefest pulse that does not exceed a specified peak–RF level. The pulse was optimized for time and constrained by a maximum gradient and maximum RF strength. The final model, parametric gradient, constrained both the maximum gradient and slew-rate, and involved the parametric gradient and the RF pulse in the objective [9]. The first two models consisted of a maximum of $3\kappa + 1$ variables, where κ was the total number of samples or RF pulses. The final model involved $\kappa(p+1)+1$ variables, where p represented a parameter vector. Experimentation proved that only 256 sample values were necessary, which kept the variable count relatively low [9]. Of the three algorithms, the parametric formulation offered the most robust SAR minimization, however, the design had areas for improvement as the results contained gradient and RF timing mismatches. Subsequently, further experimentation was necessary with VERSE pulses, as Conolly *et al.* were the first to introduce this innovative concept to the MR community.

III. The gVERSE Model

Based on the fundamental Larmor relation and the ideas proposed by Conolly *et al.* [9], we develop a new rigorous model that enhances the VERSE pulse. As previously designed, VERSE pulses perform transverse excitations while using only a fraction of the field strength in order to reduce patient heating caused by long, high energy pulses. The new gVERSE model is similar to Conolly's *et al.* in terms of constraining gradient waveform levels and slew-rate. However, the letter "g" was added to the tittle of the pulse because we allow our gradient waveform to freely vary, as we believe the addition of the gradient in the objective by Conolly *et al.* was the source of gradient–RF mismatches. As a result, we integrated the gradient in our constraints and to improve the realism of the pulse, we also introduced additional constraints to the problem. The gVERSE pulse is illustrated in Figure 3; our aim is to lower RF pulse energy and more evenly distribute the RF pulse signal. This flattened redistribution of the pulse would cause an even greater decrease in the level of SAR than the original VERSE pulse. Mathematically, this equates to minimizing the external magnetic field generated by the RF pulse ($\overrightarrow{B}_{\text{rf}}(t)$), and therefore our objective is

$$\min \text{ SAR} = \int_0^T |\overrightarrow{B}_{\text{rf}}(t)|^2 dt = \int_0^T b_x^2(t) + b_y^2(t) dt,$$

where T is the time at the end of the RF pulse and

$$\overrightarrow{B}_{\text{rf}}(t) = \begin{bmatrix} b_x(t) \\ b_y(t) \\ 0 \end{bmatrix}.$$

As MRI is based on the interaction of nuclear spin with an external magnetic field, $\overrightarrow{B}_{\text{rf}}(t)$ is simply the vertical and horizontal components of $\overrightarrow{B}(t)$. Also, if low pulse amplitudes are produced by the gVERSE pulse, the duration T of the pulse can be increased.

Another part of MRI comes from the fact that since all magnetization vectors are spinning, there exists a rotational frame of reference. However, if we set up our equations such that we are in the rotating frame of reference then we exclude the uniform magnetic field generated by the main super-conducting magnet, B_0. Instead, we are left with the magnetic field of our RF pulse, $\overrightarrow{B}_{\text{rf}}(t)$, and our gradient

$$\overrightarrow{G}(t, s) = \begin{bmatrix} 0 \\ 0 \\ sG(t) \end{bmatrix},$$

where $sG(t)$ is the gradient value at coordinate position s. The primary function of the gradient is to produce time-altering magnetic fields such that the MR signal can be spatially allocated [14]. Hence, different parts of a specimen experience different gradient field strengths. Thus, by multiplying a constant gradient value by different coordinate positions s, we have potentially produced an equivalent linear relationship to what is used in practice. Fundamentally, coordinate positions s have allowed us to split a specimen or object into "planes" or slices along the s direction, which for the purposes of this paper will be parallel to $\widehat{z}$, as depicted in Figure 4. Here, s corresponds to a specific coordinate value depending on its respective position and further it has a precise and representative gradient strength. As mentioned, an RF pulse excites particular voxels of protons into the transverse (x, y) plane where a signal is generated that is eventually processed into an image. Thus, we will use s to distinguish between voxels that are stimulated into the transverse plane by an RF pulse and those that are not. Coordinate positions, s, of voxels that are stimulated into the transverse plane will be recorded and referred to as being "in the slice." Those voxels that are not tipped into the transverse plane will be referred to as being

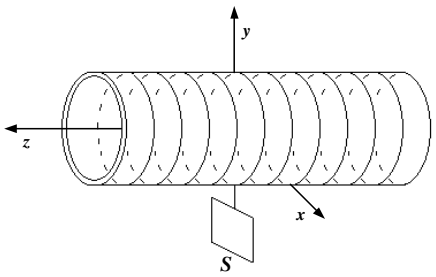

Fig. 4. Specimen or object separated into planes or slices about the z-axis.

"outside of the slice," whose respective coordinate positions, s, will also be noted. Since any specimen or object we intend to image will have a fixed length, given $s \in S$, we will restrict S by choosing a finite set $S \subset \mathbb{R}$. S can then be further partitioned into the disjoint union of sets $S_{\text{in}} \cup S_{\text{out}}$, where S_{in} represents the coordinate positions in the slice and S_{out} represents the voxels that we do not want to tip into the transverse plane, those which are outside the slice. For each coordinate position, $s \in S$, we add constraints corresponding to the Bloch equation however, boundary constraints correspond to different conditions depending on the position of the slice, as we will discuss later. Fundamentally, voxels in S_{in}, ensure uniform magnetic tipping into the transverse plane, whereas $s \in S_{\text{out}}$, certify external magnetization is preserved.

Thus, we now have $\overrightarrow{B}(t)$ with respect to coordinate positions s, whereby $b_x(t)$ and $b_y(t)$ are independent of s, hence

$$\begin{aligned}\overrightarrow{B}(t,s) &= \overrightarrow{B}_{\text{rf}}(t) + \overrightarrow{G}(t,s) \\ &= \begin{bmatrix} b_x(t) \\ b_y(t) \\ 0 \end{bmatrix} + \begin{bmatrix} 0 \\ 0 \\ sG(t) \end{bmatrix} = \begin{bmatrix} b_x(t) \\ b_y(t) \\ sG(t) \end{bmatrix}.\end{aligned}$$

Also, since $\overrightarrow{B}(t,s)$ has divided the $\widehat{z}$ component of our external magnetization into coordinate components, the same notation must be introduced into our net magnetization. Hence, by adding coordinate position s to the magnetization vector we have,

$$\overrightarrow{M}(t,s) = \begin{bmatrix} M_x(t,s) \\ M_y(t,s) \\ M_z(t,s) \end{bmatrix}.$$

In addition, since VERSE pulses typically have short sampling times we will assume the same for the gVERSE pulse and thus omit proton interactions and relaxation. Therefore, including positions s into the Bloch equation, we are left with

$$\begin{aligned}\frac{d\overrightarrow{M}(t,s)}{dt} &= \gamma \overrightarrow{M}(t,s) \times \overrightarrow{B}(t,s) \\ &= \gamma \overrightarrow{M}(t,s) \times [b_x(t), b_y(t), sG(t)]^T.\end{aligned}$$

Hence, we have

$$\begin{aligned}&\overrightarrow{M}(t,s) \times \overrightarrow{B}(t,s) \\ &= \begin{vmatrix} i & j & k \\ b_x(t) & b_y(t) & sG(t) \\ M_x(t,s) & M_y(t,s) & M_z(t,s) \end{vmatrix} \\ &= \begin{bmatrix} 0 & -sG(t) & b_y(t) \\ sG(t) & 0 & -b_x(t) \\ -b_y(t) & b_x(t) & 0 \end{bmatrix} \begin{bmatrix} M_x(t,s) \\ M_y(t,s) \\ M_z(t,s) \end{bmatrix},\end{aligned}$$

and finally

$$\frac{d\overrightarrow{M}(t,s)}{dt} = \gamma \begin{bmatrix} 0 & -sG(t) & b_y(t) \\ sG(t) & 0 & -b_x(t) \\ -b_y(t) & b_x(t) & 0 \end{bmatrix} \overrightarrow{M}(t,s). \quad (1)$$

When stimulating a specific segment of a specimen by an RF pulse, some of the magnetization vectors are fully tipped into the transverse plane, partially tipped, and those lying outside the slice are minimally affected. The magnetization vectors that are only partially tipped into the transverse plane are described as having off-resonance and tend to disrupt pulse sequences and distort the final MRI image [14]. In anticipation of removing such in-homogeneities we introduce the angle α, at which net magnetization moves from the $\widehat{z}$ direction to the transverse plane. By convention, α will be the greatest at the end of our RF pulse, at time T, and since we are in the rotating frame we can remove the y-axis from our equations. Thus, we can eliminate off-resonance s coordinates by bounding voxels affected by the pulse

$$\left\| \begin{bmatrix} M_0 \sin(\alpha) \\ 0 \\ M_0 \cos(\alpha) \end{bmatrix} - \begin{bmatrix} M_x(T,s) \\ M_y(T,s) \\ M_z(T,s) \end{bmatrix} \right\| \leq \varepsilon_1,$$

and those not affected by the pulse, with $\alpha = 0$, hence

$$\left\| \begin{bmatrix} 0 \\ 0 \\ M_0 \end{bmatrix} - \begin{bmatrix} M_x(T,s) \\ M_y(T,s) \\ M_z(T,s) \end{bmatrix} \right\| \leq \varepsilon_2,$$

where $\varepsilon_1, \varepsilon_2 \geq 0$. Therefore, by comparing these two bounds we can determine the s coordinates from which we would like the signal to be generated and exclude off-resonance.

Another factor we must integrate into our pulse is slew rate, $W(t)$, also called gradient-echo rise time. This identifies how fast a magnetic gradient field can be ramped to different gradient field strengths [9]. As a result, higher slew rates enable shorter measurement times since the signal generated by the RF pulse to be imaged is dependent on it. Thus, the slew rate and gradient field strength together determine an upper bound on the speed and ultimately minimum time needed to perform the pulse. Thus, there must be a bound on these two entities in our constraints,

$$\begin{aligned}|G(t)| &\leq G_{\max}, \\ W(t) = \left| \frac{dG(t)}{dt} \right| &\leq W_{\max}.\end{aligned}$$

Finally, we have the semi-infinite nonlinear optimization problem

$$\min \text{ SAR} = \int_0^T b_x^2(t) + b_y^2(t) dt, \quad (2)$$

subject to,

$$\frac{d\overrightarrow{M}(t,s)}{dt} = \gamma \begin{bmatrix} 0 & -sG(t) & b_y(t) \\ sG(t) & 0 & -b_x(t) \\ -b_y(t) & b_x(t) & 0 \end{bmatrix} \overrightarrow{M}(t,s), \quad (3)$$

$$\left\| \begin{bmatrix} M_0 \sin(\alpha) \\ 0 \\ M_0 \cos(\alpha) \end{bmatrix} - \begin{bmatrix} M_x(T,s) \\ M_y(T,s) \\ M_z(T,s) \end{bmatrix} \right\| \leq \varepsilon_1, \qquad (4S_{\text{in}})$$

$$\left\| \begin{bmatrix} 0 \\ 0 \\ M_0 \end{bmatrix} - \begin{bmatrix} M_x(T,s) \\ M_y(T,s) \\ M_z(T,s) \end{bmatrix} \right\| \leq \varepsilon_2, \qquad (4S_{\text{out}})$$

$$|G(t)| \leq G_{\max}, \qquad (5)$$

$$\left| \frac{dG(t)}{dt} \right| \leq W_{\max}, \qquad (6)$$

$$M_x(0,s) = 0, \quad M_y(0,s) = 0, \quad M_z(0,s) = M_0, \qquad (7)$$

where equations (2) – (7) hold for $\forall\, s \in S, t \in [0,T]$. Expanding the first constraint (3) produces the following equations,

$$\frac{dM_x(t,s)}{dt} = \gamma[-sG(t)M_y(t,s) + b_y(t)M_z(t,s)], \qquad (8)$$

$$\frac{dM_y(t,s)}{dt} = \gamma[sG(t)M_x(t,s) - b_x(t)M_z(t,s)], \qquad (9)$$

$$\frac{dM_z(t,s)}{dt} = \gamma[-b_y(t)M_x(t,s) + b_x(t)M_y(t,s)]. \qquad (10)$$

Thus, depending on our bound for the pulse, we will construct two sets of constraints, one for the voxels $S_{\text{in}} \subset \mathbb{R}$ that will be stimulated by the RF pulse and one for those that will not, $S_{\text{out}} \subset \mathbb{R}$. Which indices are affected will be determined by constraints ($4S_{\text{in}}$) and ($4S_{\text{out}}$). Thus, if we are given the voxels, ($4S_{\text{in}}$) our pulse affects, then we can apply equations (8), (9) and (10) respectively. The same can be done for the other set of voxels minimally affected by the RF pulse, S_{out}.

A. Discretization

By separating our specimen into coordinate positions we have ultimately created two dimensional segments that are similar to records in a record box, whereby $s \in S$ represents the transverse plane at a particular position. Now we will discretize S into coordinate positions $s_1, s_2, \ldots, s_n$, where n is the total number of slices. Previously we defined S_{in} as the coordinate positions whose voxels have been tipped into the transverse plane by an RF pulse. Now S_{in} will consist of a finite band of particular coordinate positions whose magnetization vectors have been excited into the transverse plane, hence, $S_{\text{in}} = s_k, \ldots, s_{k+\delta}$, where $1 < k \leq k+\delta < n$, $\delta \geq 0$ and $k, \delta \in \mathbb{Z}$. Subsequently S_{out}, which was defined as positions that were not stimulated in the transverse plane, will consist of all coordinate positions not in S_{in}, thus, $S_{\text{out}} = s_1, \ldots, s_{k-1}, s_{(k+\delta)+1}, \ldots, s_n$. Figure 5 represents how $s_i \in S$ for $i = 1, \ldots, n$ would separate magnetization vectors into coordinate positions that have been tipped into the transverse plane, and those that have not. One should also note that we have only discretized with respect to coordinate positions $s_i \in S$, not time t. Furthermore, we will define the first coordinate position in S_{in} where RF pulse stimulation begins as $\underline{s}$, and similarly, the last position in S_{in} where stimulation ends as $\overline{s}$. Thus, we have $\underline{s} = s_k$ and $\overline{s} = s_{k+\delta}$, and we can now state the coordinate positions in the slice as $S_{\text{in}} = [\underline{s}, \overline{s}]$. The first position where RF stimulation is a minimum, closest to $\underline{s}$, but in S_{out} and towards the direction of s_1, will be defined as $\underline{s}_l$. As well, the same will be done for the position closest to $\overline{s}$, which is in S_{out} and towards the direction of s_n, defined as $\overline{s}_u$. Consequently, $\underline{s}_l = s_{k-1}$ and $\overline{s}_u = s_{(k+\delta)+1}$, and therefore the coordinate positions outside the slice can be represented as $S_{\text{out}} = [s_1, \underline{s}_l] \cup [\overline{s}_u, s_n]$. As depicted in Figure 5, S_{in} is located between the two subintervals of S_{out}, where $s_i \in S_{\text{in}}$ is centered around 0, leaving S_{out} subintervals, $[s_1, \underline{s}_l] < 0$ and $[\overline{s}_u, s_n] > 0$. As well, $[s_1, \underline{s}_l]$ and $[\overline{s}_u, s_n]$ are symmetric with respect to each other, hence, the length of these subintervals are equivalent, $s_{k-1} - s_1 = s_n - s_{(k+\delta)+1}$. Furthermore, the difference between respective coordinate positions within each interval are equal to one another such that,

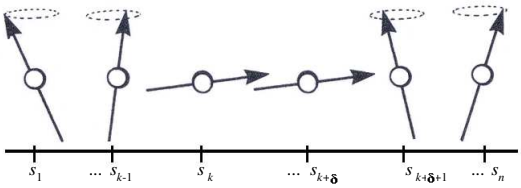

Fig. 5. Separating magnetization vectors into coordinate positions which are in the slice, S_{in}, and out, S_{out}.

$$\begin{aligned} s_2 - s_1 &= s_n - s_{n-1} \\ s_3 - s_2 &= s_{n-1} - s_{n-2} \\ \vdots \qquad &\qquad \vdots \\ s_{k-1} - s_{k-2} &= s_{(k+\delta)+2} - s_{(k+\delta)+1}. \end{aligned} \qquad (11)$$

Also note that the discretization points, s_i, within any interval $[s_1, \underline{s}_l], [\underline{s}, \overline{s}]$ and $[\overline{s}_u, s_n]$ do not necessarily have to be uniformly distributed and thus, more coordinate positions could be positioned closer to the boundaries of S_{in} and S_{out}. The distance between coordinate positions $(\underline{s}_l, \underline{s})$ and $(\overline{s}, \overline{s}_u)$ will be much larger in comparison to other increments of s_i. This is typically the area where voxels that have off-resonance characteristics are located. As mentioned earlier, magnetization vectors having off-resonance tend to disrupt pulse sequences and distort the MRI image. For this reason we will define the tolerance gaps of finite length where off-resonance prominently resides, between $(\underline{s}_l, \underline{s})$ and $(\overline{s}, \overline{s}_u)$, as S_0. Hence, S can now be partitioned into $S_{\text{in}} \cup S_{\text{out}} \cup S_0$ where a general sequence of the intervals would be $S_{\text{out}}, S_0, S_{\text{in}}, S_0, S_{\text{out}}$.

B. gVERSE Penalty

An important component of the model now becomes evident, the nonlinear optimization problem defined in (2) – (7) may be infeasible or difficult to solve when the number n of $s_i \in S$ becomes large and the slices are close together. In particular, constraints ($4S_{\text{in}}$) and ($4S_{\text{out}}$) potentially pose a threat to the feasibility of the problem as the number of

discretization points increase. A penalty for the violation of these constraints can be imposed such that an optimal solution is located for problems with large numbers of variables and small distances between s_i coordinate positions. The basic idea in penalty methods is to relax particular constraints and add a penalty term to the objective function that prescribes high cost to infeasible points [1]. The penalty parameter determines the severity of violation and as a consequence, the extent to which the resulting unconstrained problem approximates the original constrained one. Thus, returning to the semi-infinite nonlinear optimization problem formulated at the start of Section III, we introduce penalty variables ξ_1 and ξ_2 to constraints ($4S_{\text{in}}$) – ($4S_{\text{out}}$), and the optimization problem objective becomes,

$$\min \text{ SAR} = \int_0^T b_x^2(t) + b_y^2(t)\, dt + \xi_1\zeta_1 + \xi_2\zeta_2, \qquad (12)$$

subject to constraints (3), (5) – (7), and

$$\left\| \begin{bmatrix} M_0\sin(\alpha) \\ 0 \\ M_0\cos(\alpha) \end{bmatrix} - \begin{bmatrix} M_x(T,s_i) \\ M_y(T,s_i) \\ M_z(T,s_i) \end{bmatrix} \right\| \leq \varepsilon_1 + \xi_1, \quad (13S_{\text{in}})$$

$$\left\| \begin{bmatrix} 0 \\ 0 \\ M_0 \end{bmatrix} - \begin{bmatrix} M_x(T,s_i) \\ M_y(T,s_i) \\ M_z(T,s_i) \end{bmatrix} \right\| \leq \varepsilon_2 + \xi_2, \quad (13S_{\text{out}})$$

where $\zeta_1, \zeta_2 \in \mathbb{R}$ are scalar penalty parameters and as earlier, equations (12) – ($13S_{\text{out}}$) apply $\forall\, s \in S, t \in [0,T]$. One should note that the larger the value of ζ_1 and/or ζ_2, the less violated constraints ($13S_{\text{in}}$) and/or ($13S_{\text{out}}$) become. In addition, as it is written, the penalty variables are applied to each $s_i \in S$ for constraints ($13S_{\text{in}}$) and ($13S_{\text{out}}$). However, depending on computational results, it may be appropriate to only penalize coordinate positions in the neighbourhood of the bounds $[\underline{s}_l, \underline{s}]$ and $[\overline{s}, \overline{s}_u]$. This would enhance the constraints on the optimization problem and only allow violations to occur at the most vulnerable points of the problem. Adding penalty variables and parameters to our optimization problem is an option that may not be necessary. It is dependent on the number n of coordinate positions applied to the model as well as, how close we would like $s_i \in S$ to be to one another. Hence, for the remainder of this paper we will omit writing out the penalty variables and parameters, however, the reader should note that they can easily be incorporated into the formulation.

IV. Implementation

The Sparse Optimal Control Software ($\mathbb{SOCS}$) package from The Boeing Company was used to solve the nonlinear gVERSE pulse problem. First, it was necessary to convert the NLO from (2) – (7) into an optimal control problem. An optimal control problem is simply an infinite-dimensional extension of an NLO problem. In fact, practical methods for solving optimal control problems require iterations with a finite set of variables and constraints [4]. Typically, optimal control problems are formulated as a collection of state, control and independent variables. By definition, state variables act collectively as the trajectory of the system, whereas, control variables determine the course of the process [7]. For the gVERSE pulse problem the state and control variables are defined within the dynamics of the system. Thus, for a problem with n slices, the state variables are defined by a $3n+1$ dimensional state vector

$$\Omega(t) = [M_x(t,s_1), M_y(t,s_1), M_z(t,s_1), \ldots, M_x(t,s_n), M_y(t,s_n), M_z(t,s_n), G(t)]^T,$$

where $\Omega(t) \in \mathbb{R}^{3n+1}$. Similarly, the three dimensional control vector is

$$\Phi(t) = [b_x(t), b_y(t), W(t)]^T$$

with $\Phi(t) \in \mathbb{R}^3$. Subsequently, for any gVERSE pulse problem we solve, the total number of state and control variables are $3n+4$. Our system is governed by differential equations (8), (9), (10) and slew rate, where for $i = 1, \ldots, n$ we have

$$\begin{aligned}
\frac{dM_x(t,s_i)}{dt} &= \gamma[-s_i G(t) M_y(t,s_i) + b_y(t) M_z(t,s_i)], \\
\frac{dM_y(t,s_i)}{dt} &= \gamma[s_i G(t) M_x(t,s_i) - b_x(t) M_z(t,s_i)], \\
\frac{dM_z(t,s_i)}{dt} &= \gamma[-b_y(t) M_x(t,s_i) + b_x(t) M_y(t,s_i)], \\
\frac{dG(t)}{dt} &= W(t).
\end{aligned}$$

This can then be represented as a function of state and control variables, namely

$$f\big(\Omega(t), \Phi(t)\big) = \begin{bmatrix} \frac{dM_x(t,s_1)}{dt} \\ \frac{dM_y(t,s_1)}{dt} \\ \frac{dM_z(t,s_1)}{dt} \\ \vdots \\ \frac{dM_x(t,s_n)}{dt} \\ \frac{dM_y(t,s_n)}{dt} \\ \frac{dM_z(t,s_n)}{dt} \\ \frac{dG(t)}{dt} \end{bmatrix}, \qquad (14)$$

where $f\big(\Omega(t), \Phi(t)\big)$ is a $3n+1$ dimensional vector. In addition, the solution must also satisfy path constraints $G(t)$ and $W(t)$. For our problem bounds can be imposed on the state and control variables,

$$-G_{\max} \leq G(t) \leq G_{\max} \qquad (15)$$

$$-W_{\max} \leq W(t) \leq W_{\max}, \qquad (16)$$

which pertains to constraints (5) and (6), respectively. Therefore, we will define our path constraints by the vector

$$\Psi\big(\Omega(t), \Phi(t)\big) = \begin{bmatrix} G(t) \\ W(t) \end{bmatrix}, \qquad (17)$$

which satisfies

$$\Psi_L \leq \Psi\big(\Omega(t), \Phi(t)\big) \leq \Psi_U, \qquad (18)$$

where

$$-\Psi_L = \Psi_U = \begin{bmatrix} G_{\max} \\ W_{\max} \end{bmatrix}.$$

In anticipation of finding an optimal solution, boundary conditions define the values of particular state variables at the start and end time of our evaluation. This allows the value of the dynamic variables at the beginning and end of our time interval to be pre-defined [4]. Thus, the initial conditions at the start of the time interval, $t = 0$, are

$$M_x(0, s_i) = 0, \tag{19}$$
$$M_y(0, s_i) = 0, \tag{20}$$
$$M_z(0, s_i) = M_0, \tag{21}$$

again for $i = 1, \ldots, n$. Hence, the values from (19) – (21) are entered into $\Omega(0)$ at the beginning of our evaluation. Terminal conditions that must be satisfied at the end of the time interval are different for magnetization vectors in S_{in}, then for those in S_{out}. As depicted in constraints ($4S_{\text{in}}$) and ($4S_{\text{out}}$), at the end of our time interval, $t = T$, the terminal condition for the voxels $s_i \in S_{\text{in}}$ are,

$$-\varepsilon_1 \leq \begin{bmatrix} M_0 \sin(\alpha) \\ 0 \\ M_0 \cos(\alpha) \end{bmatrix} - \begin{bmatrix} M_x(T, s_i) \\ M_y(T, s_i) \\ M_z(T, s_i) \end{bmatrix} \leq \varepsilon_1. \tag{22}$$

Whereas, for voxels $s_i \in S_{\text{out}}$, we have the following terminal condition,

$$-\varepsilon_2 \leq \begin{bmatrix} 0 \\ 0 \\ M_0 \end{bmatrix} - \begin{bmatrix} M_x(T, s_i) \\ M_y(T, s_i) \\ M_z(T, s_i) \end{bmatrix} \leq \varepsilon_2. \tag{23}$$

Subsequently, the values for (22) and (23) are entered into $\Omega(T)$ at the end of the evaluation. Thus, the boundary conditions for the gVERSE pulse problem will be expressed by

$$\psi_L \leq \psi\big(\Omega(t), \Phi(t)\big) \leq \psi_U, \tag{24}$$

where ψ_L and ψ_U contain the respective initial and terminal condition values found in (19) – (23). Penalty variables ξ_1 and ξ_2 would be incorporated into (22) and (23), respectively, if the problem required penalty terms. Also note that equality constraints can be imposed by using inequality ones by simply setting upper and lower bounds equal to one another, i.e., $\psi_L = \psi_U$. Finally, our objective function to be minimized will be expressed as

$$\int_0^T w\big(\Phi(t)\big)\, dt = \int_0^T b_x^2(t) + b_y^2(t)\, dt, \tag{25}$$

where $w\big(\Phi(t)\big)$ is known as the quadrature function, which is commonly found in optimal control literature [5]. If penalty was part of our problem then $\xi_1\zeta_1$ and $\xi_2\zeta_2$ would be added to the quadrature function in (25). Collectively, we refer to the functions evaluated during the time interval as

$$F(t) = \begin{bmatrix} f\big(\Omega(t), \Phi(t)\big) \\ \Psi\big(\Omega(t), \Phi(t)\big) \\ w\big(\Phi(t)\big) \end{bmatrix}, \tag{26}$$

the vector of continuous functions, however, boundary conditions evaluated at specific points are referred to as point functions [5]. Therefore, the solution to the optimal control problem requires

$$J(t) = \int_0^T w\big(\Phi(t)\big)\, dt \tag{27}$$

to be minimized.

Once the explicit details of the optimal control formulation have been established, it is then possible to solve the gVERSE pulse problem after the independent time variable has been discretized. Thus, time t is divided into N discretization points over the interval $[0, T]$, including the end points. Hence, the time discretizations are as follows:

$$0 = t_1 < t_2 < \ldots < T = t_N.$$

For more information on how an NLO is transformed into an optimal control problem the reader may consult [4], [5].

A. Slice Assignment

In the gVERSE model constructed in Section III *A*, S was discretized into coordinate positions $s_1, s_2, \ldots, s_n$ and partitioned into the sets S_{in} and S_{out}. Furthermore, the coordinate positions in S_{in} were bounded by $[\underline{s}, \overline{s}]$, and S_{out} was composed of coordinate positions in $[s_1, \underline{s}_l]$ and $[\overline{s}_u, s_n]$. More specifically, $\underline{s}_l = s_{k-1}$, $\underline{s} = s_k$, $\overline{s} = s_{k+\delta}$ and $\overline{s}_u = s_{k+\delta+1}$, for $1 < k \leq k + \delta < n$ and $\delta \geq 0$. Thus, for an application with n slices, each $s_i \in S$ was given a scalar value defined by

$$s_i = \begin{cases} \underline{\beta} + \rho_1(i) & i \leq k-1, \\ \beta + \rho_2(i) & k \leq i \leq k+\delta, \\ \overline{\beta} + \rho_3(i) & i \geq (k+\delta)+1, \end{cases} \tag{28}$$

where $\underline{\beta}, \beta, \overline{\beta} \in \mathbb{R}$. In order to include the off-resonance characteristics found between $(\underline{s}_l, \underline{s})$ and $(\overline{s}, \overline{s}_u)$, the formula in (28) is designed such that $\underline{\beta} + \rho_1(k-1) < \beta \leq \beta + \rho_2(k+\delta) < \overline{\beta}$. Also, $\rho_1(i), \rho_2(i), \rho_3(i)$ are strictly monotonically increasing functions that can uniformly or randomly disperse increments of s_i. As stated in Section III *A*, the subinterval $[\underline{s}, \overline{s}]$ is intended to be centered around 0, and hence, β is chosen such that $\beta + \rho_2(i)$ has the same features for $k \leq i \leq k + \delta$. Also, the values, $\underline{\beta} < 0$ and $\overline{\beta} > 0$, are assigned such that the positions $\underline{\beta} + \rho_1(i)$ for $i \leq k-1$ and $\beta + \rho_3(i)$ for $i \geq (k+\delta)+1$ are symmetric with respect to each other, as shown in (11). Therefore, using this construction, $\beta + \rho_2(i)$ will contain the values for the magnetization vectors in S_{in}, whereas, $\underline{\beta} + \rho_1(i)$ and $\overline{\beta} + \rho_3(i)$ will control the $s_i \in S_{\text{out}}$ values. The initial positions, $\underline{\beta}, \beta, \overline{\beta}$, for this piecewise step function will be chosen depending on how many slices, n, we have and how far we would like to disperse our RF pulse. For example, generally we would assign values such that $\underline{\beta} \approx s_1$, $\beta \approx s_k$ and $\overline{\beta} \approx s_{(k+\delta)+1}$. Also notice, we can set the distance between $\underline{\beta} + \rho_1(k-1) < \beta$ and $\beta + \rho_2(k+\delta) < \overline{\beta}$ or S_0 to be as large as we like. Thus, potentially controlling the negative imaging effects described in Section III, which

are experienced by off-resonance magnetization vectors found in these positions.

After the slices were separated into the sets S_{in} and S_{out} with appropriate values, they were ready to be evaluated within constraints (3) – (7). At $t_1 = 0$, the values of $M_x(0, s_i)$, $M_y(0, s_i)$ and $M_z(0, s_i)$ were initialized for $i = 1, \ldots, n$ in an input routine. In the next section we will show how a guess subroutine of the initial solution is efficiently used to estimate $M_x(t_j, s_i)$, $M_y(t_j, s_i)$ and $M_z(t_j, s_i)$ for $t_j \in (t_1, t_N)$, $s_i \in [s_1, s_n]$.

B. Initial Solution

A softwares efficiency and robustness in solving a nonlinear problem can be improved by the addition of an intelligent initial guess to the solution of the problem. Even finding a feasible starting point can be difficult with NLO problems, re-emphasizing the importance of our initial solution implemented in $\mathbb{SOCS}$ as a guess subroutine. In the gVERSE problem, we understand how the magnetization vectors

$$[M_x(t_j, s_1), M_y(t_j, s_1), M_z(t_j, s_1)]^T, \\ \ldots, [M_x(t_j, s_n), M_y(t_j, s_n), M_z(t_j, s_n)]^T$$

physically behave in vivo. Also, a generic RF pulse design can be utilized to hypothesize what the values of $G(t_j), b_x(t_j)$ and $b_y(t_j)$ could be. Thus, for these variables we supplied a subroutine that defined the initial guess of the solution to our optimal control problem. We begin by describing how the algorithm was coded for the n magnetic moment vectors and follow with the gradient and external magnetization components.

The input for values of the n magnetic moment vectors, $M_x(t_j, s_i), M_y(t_j, s_i)$ and $M_z(t_j, s_i)$, were different depending on whether $s_i \in S_{\text{in}}$ or $s_i \in S_{\text{out}}$. For the vectors that were in S_{in}, our initial guess subroutine was required to tip $[M_x(t_j, S_{\text{in}}), M_y(t_j, S_{\text{in}}), M_z(t_j, S_{\text{in}})]^T$ into the transverse plane by an angle of α. However, if $s_i \in S_{\text{out}}$, then these vectors were required to be in the direction of the static external magnetic field, B_0, which as mentioned earlier is parallel to the z-axis. Therefore, the algorithm for the initial guess of the vectors in S_{in} would follow Figure 6, where these voxels were set to tip into the transverse plane by an angle of α at the end of the time duration t_N. Magnetic moment vectors in S_{out}, however, would align in the z-axis direction with a height of M_0. To produce high quality MR final images, this is exactly what we would like to observe in terms of magnetic moment vectors.

With regards to gradient and external magnetization, a generic RF pulse sequence similar to the one shown in Figure 1 was used to infer how our initial solution for these variables were modelled. In doing so, the upper plot in Figure 7 illustrates how our gradient function, $G(t)$, behaved. There are a few important characteristics of the gradient function worth mentioning. The most significant is that the two areas, highlighted by diagonal lines, are equivalent. Specifically, the area between points g_1 to g_3 is equal to that of g_5 to g_8, where g_3 is the midpoint of g_2 and g_4. Another important element of the gradient function is that the absolute value of

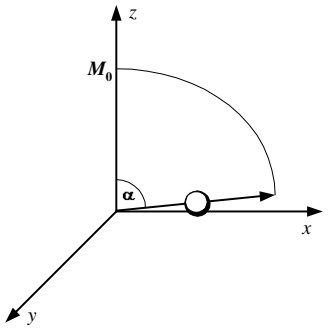

Fig. 6. The initial solution for magnetic moment vectors in S_{in} that have tipped into the transverse plane by an angle of α.

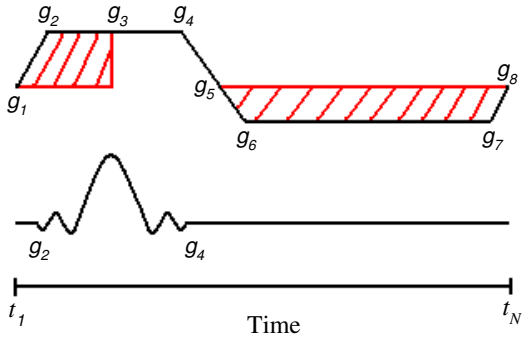

Fig. 7. The initial solution for the gradient function $G(t)$ (top) and external magnetization $b_y(t)$ (bottom).

the slope of these lines be less than or equal to the maximum slew rate, W_{max}. Finally, the absolute value of the hight of the lines, g_2 to g_4 and g_6 to g_7, are required to be less than or equal to the maximum gradient, G_{max}. To implement such a function, a simple program in Maple, symbolic mathematics software produced by Maplesoft, was created that would list the possible values for g_1 to g_8 that satisfy the above criteria. One can easily deduce from Figure 7 that the values for $g_1, \ldots, g_8$ will correspond to specific time discretizations, t_j, within the interval t_1 to t_N. Hence, when the time values of $g_1, \ldots, g_8$ have been determined, including the slope from g_1 to g_2, and the value of both lines, g_2 to g_4 and g_6 to g_7, the gradient function was then implemented.

For the values of the external magnetization variables, a standard RF pulse was used. Generally, $b_x(t)$ remains constant and is zero, however, $b_y(t)$ behaves similar to the lower plot in Figure 7. In the illustration, the value of g_2 and g_4 correspond to vales that were determined in the gradient function. Using this model for our guess function, we have created an intelligent approximation of how the variables defined within the problem should behave.

V. Results

The gVERSE pulse was precisely designed to improve RF pulse sequences by minimizing SAR and enhancing MRI

resolution. The complex mathematical requirements of the gVERSE model may be difficult to satisfy, even simple NLO problems with large numbers of variables can be challenging to solve and threatens many software packages. Thus, when attempting to minimize the objective function in (2) under the constraints (3) – (7), the number of variables implemented was especially important. Preliminary results were found by implementing the gVERSE model using five coordinate positions. This kept the variable count to a minimum of 19, $(3n + 4)$, excluding the independent time variable, t. The number of variables was systematically increased to 49, until software limitations on memory became a factor. Nonetheless, this was a remarkably larger number of variables than anticipated, as it accounted for 15 slices with a total of 38 857 variables, after time discretizations were made. By experimenting and consulting the literature, realistic MRI values for the constants were used during each computational simulation. Namely, $\gamma = 42.58$ Hz/mT, $G_{\text{max}} = 0.02$ mT/mm and $W_{\text{max}} = 0.2$ mT/mm/ms, where Hz is Hertz, mm is millimeters, ms is milliseconds, and mT is millitelsa. The magnetization vectors in S_{in} were fully tipped into the transverse plane, hence, $\alpha = \frac{\pi}{2}$. The magnitude of the initial magnetization vector for each coordinate position had an initial magnetization value of $M_0 = 1.0$ spin density units. Initially, we chose $\varepsilon_1, \varepsilon_2 \leq 0.1$, however, as the number of variables increased for the problem, the larger the value of ε_1 and ε_2 had to be in order to find a feasible solution, hence, $\varepsilon_1, \varepsilon_2 = 0.1$ for the 15 slice results.

A. Fifteen slice Results

The results for the 15 slice problem accounted for the largest number of variables that $\mathbb{SOCS}$ could solve. The problem became even more challenging as the distance from $\underline{s}$ to $\overline{s}$ increased. For large distances between the magnetization vectors in S_{in} penalty variables and parameters had to be incorporated into the formulation of the problem. We will begin with the 15 slice results without penalty, where a shorter distance between $\underline{s}$ and $\overline{s}$ was used.

Since there were 15 slices, the three middle magnetization vectors were tipped into the transverse plane to ensure that the symmetric structure of the problem was maintained. Hence, coordinate positions s_7, s_8 and s_9 were in S_{in}, while $s_1, s_2, \ldots s_6$ and $s_{10}, s_{11}, \ldots s_{15}$ remained in S_{out}. The arrangement of the coordinate positions is shown in Figure 8 and the exact values for the coordinate positions are as follows:

$$\begin{array}{cccccc} -30 & -28 & -26 & -24 & -22 & -20 \\ s_1 & s_2 & s_3 & s_4 & s_5 & s_6 \end{array}$$
$$\begin{array}{ccc} -0.2 & 0 & 0.2 \\ s_7 & s_8 & s_9 \end{array}$$
$$\begin{array}{cccccc} 20 & 22 & 24 & 26 & 28 & 30 \\ s_{10} & s_{11} & s_{12} & s_{13} & s_{14} & s_{15} \end{array}$$

which is in mm. The results for the 15 slice coordinate simulation is illustrated in Figures 9, 10 and 13. Information on the magnetic vector projection is shown in the graphs found in Figures 9 – 10. Due to the symmetric structure of the problem, voxels $s_1, \ldots, s_6$ and $s_{10}, \ldots, s_{15}$ were identical, as were s_7 and s_9. Hence, only the first eight coordinate positions are shown. Thus, Figure 9 – 10 corresponds to magnetization vectors in S_{out} and S_{in}. The resulting RF pulse procedure, represented by the external magnetization components and the gradient waveform is shown in Figure 13; $b_x(t)$ is not shown as it was constant and equal to zero.

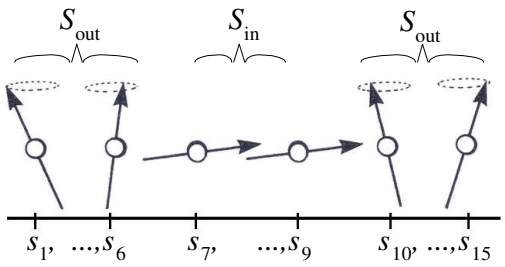

Fig. 8. The separation of coordinate positions s_i into S_{in} and S_{out} for 15 magnetization vectors.

One can observe that the precession of the magnetization vectors in S_{out} is evident, this is shown in the graphs of Figure 9 – 10. The initial point is close to the voxels precession range and at most it takes one full rotation for them to orbit uniformly. The magnetization vectors in Figure 10, those s_i that belong to S_{in}, smoothly tip into the transverse plane without any cusps or peaks. There are small differences between s_7 and s_8 as they begin to tip into the transverse plane, however, they act very similar after their height decreases below 0.8 spin density units. In Figure 13, the gradient waveform starts off negative and then ends up positive. It is not a smooth curve since it is composed of many local hills and valleys. Also, the gradient seems to be the opposite of what is used in practical MRI sequences (shown in Figure 7), however this proves to be a proficient sequence as we will investigate in the next Section. Finally, the external magnetization components, $b_x(t)$ and $b_y(t)$, are constant and linear, precisely what we optimized for in the objective function. The value of $b_x(t)$ is zero mT/mm, while $b_y(t)$ of Figure 13 has a constant value of 0.01925 mT/mm.

B. Fifteen Slice Penalty Results

To increase the distance between the coordinate positions that were tipped into the transverse plane and allow a smooth transition between magnetization vectors in S_{in} and S_{out}, penalty variables and parameters were introduced. Initially, penalty variables were only integrated into the constraints corresponding to coordinate positions that were close to the border of S_{in} and S_{out}, as described in Section III *B*. However, for the 15 slice problem, when penalty variables ξ_1 and ξ_2 were only added to constraints pertaining to s_i in a neighbourhood of $[\underline{s}_l, \underline{s}]$ and $[\overline{s}, \overline{s}_u]$, no feasible solution was found. In fact, in order to increase the distance between s_7 and s_9 penalty variables had to be incorporated to each s_i vector in constraints $(13S_{\text{in}})$ and $(13S_{\text{out}})$. The remaining variables, constants, and constraints were consistent with what was used in the other results. The exact values for the coordinate positions were as

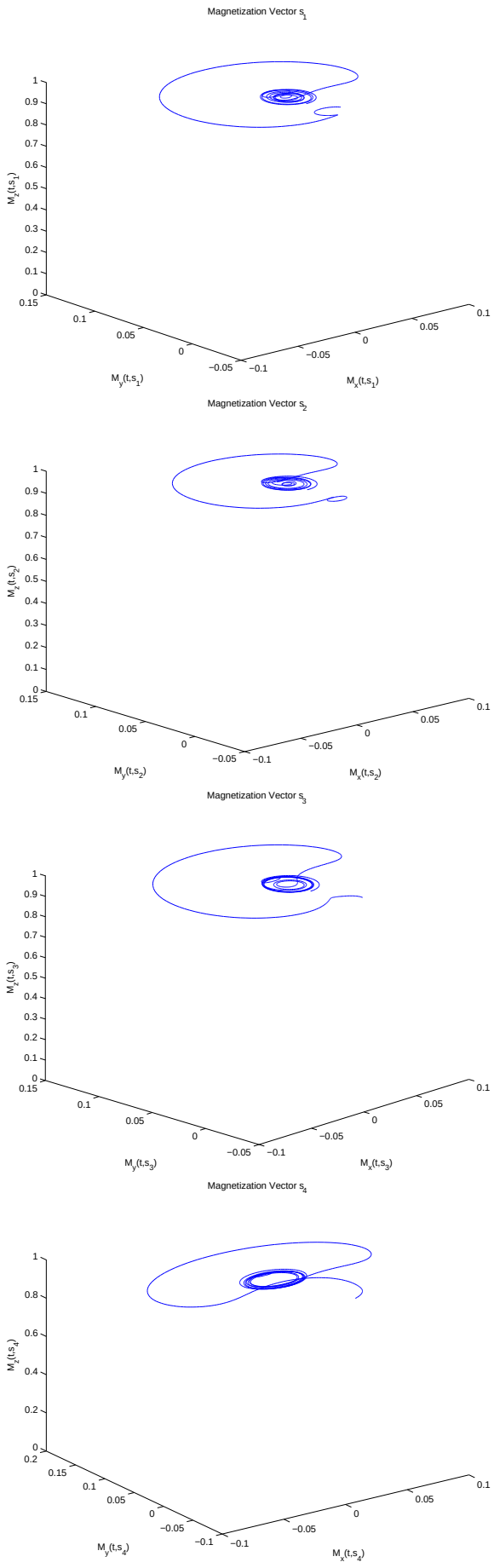

Fig. 9. From Top to bottom, magnetization vectors corresponding to coordinate positions s_1, s_2, s_3 and s_4.

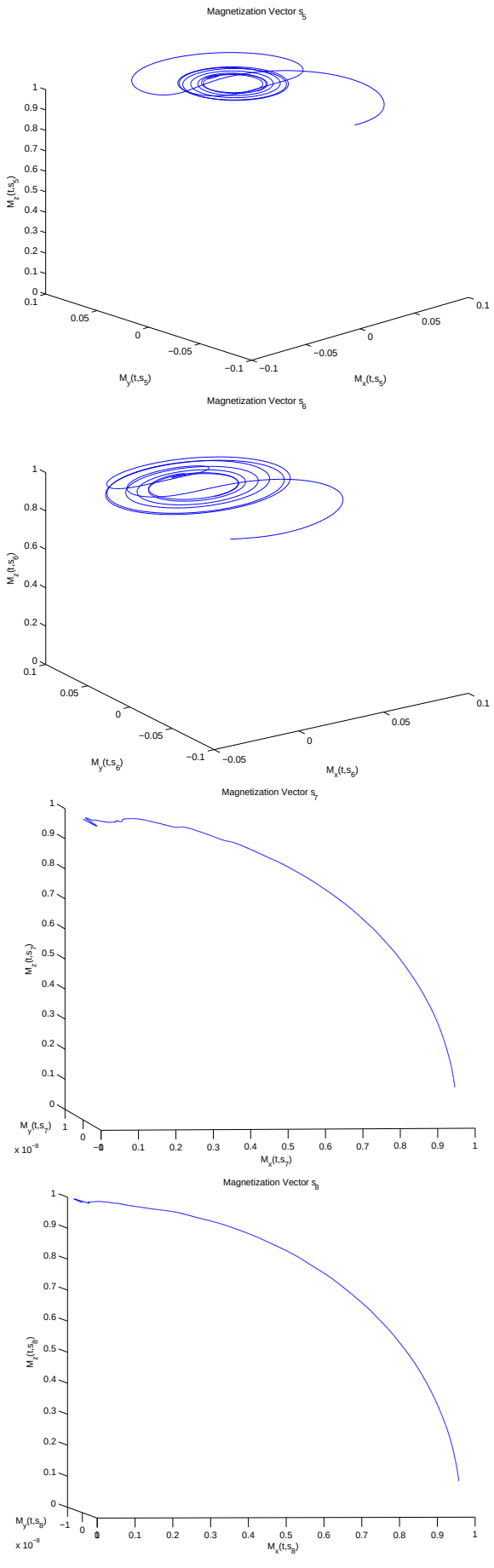

Fig. 10. From top to bottom, magnetization vectors corresponding to coordinate positions s_5, s_6, s_7 and s_8.

follows:

$$\begin{array}{cccccccccccc} -30 & -28 & -26 & -24 & -22 & -20 \\ s_1 & s_2 & s_3 & s_4 & s_5 & s_6 \\ \xi_2 & \xi_2 & \xi_2 & \xi_2 & \xi_2 & \xi_2 \\ & & -2 & 0 & 2 & \\ & & s_7 & s_8 & s_9 & \\ & & \xi_1 & \xi_1 & \xi_1 & \\ 20 & 22 & 24 & 26 & 28 & 30 \\ s_{10} & s_{11} & s_{12} & s_{13} & s_{14} & s_{15} \\ \xi_2 & \xi_2 & \xi_2 & \xi_2 & \xi_2 & \xi_2 \end{array}$$

where the positions that were penalized have their respective penalty variables listed below them. Notice that, with the addition of penalty variables and parameters the distance from s_7 to s_9 increased to 4 mm, compared to the 0.4 mm difference in the 15 slice results on page 10. Also, in the implementation of the penalized optimization problem from (12) – (13S_{out}), the value of the penalty parameters could not exceed, $\zeta_1 = 100$ and $\zeta_2 = 100$. The results for the penalized 15 coordinate simulation is illustrated in Figures 11, 12 and 14. Information on the magnetic vector projection is shown in the graphs found in Figure 11 – 12. Again, due to the problems symmetry we have omitted the graphs of magnetization vectors corresponding to coordinate positions $s_9, \ldots, s_{15}$. Hence, Figure 11 and the top two graphs in 12 correspond to magnetization vectors in S_{out}, whereas the bottom two graphs in Figure 12 refer to the coordinate positions in S_{in}. The resulting RF pulse procedure, represented by the external magnetization components and gradient sequence is shown in Figure 14; again $b_x(t)$ is not shown as it was constant and equal to zero.

As illustrated, the precession of the magnetization vectors in S_{out}, Figure 11 – 12, have a much larger radius than that of the 15 slice problem. In fact, these magnetization vectors have at most three successive orbits in the entire time duration. The magnetization vectors in Figure 12, those s_i that belong to S_{in}, smoothly tip into the transverse plane and there is a greater similarity between s_7 and s_8 than in the preceding results. However, due to the penalty variables these vectors do not tip down as far into the transverse plane, to approximately a spin density value of 0.2. Also, the y-axis is larger than the 15 slice problem, this is because the $M_y(t, \cdot)$ component of these magnetization vectors is increasing as they are descending into the transverse plane. In Figure 14, the gradient waveform is more linear than the last result. It contains two large peaks, the first is negative and it starts about one quarter into the time period. The second peak is positive and it starts approximately three quarters into the time period. Also, the gradient sequence has three linear segments. One that is zero at the start of the sequence and the other two occur within the peaks, each having a value of exactly $\pm G_{\text{max}}$. For the external magnetization components, $b_x(t)$ is again constant and has a value of zero mT/mm. Although the axis of $b_y(t)$ in Figure 14 has been magnified, it is not as linear as the previous results and has increased to a value of approximately 0.10116 mT/mm. Nevertheless, this is still less than the amplitude for a conventional pulse, such as the one illustrated in Figure 1, which has a typical $b_y(t)$ value of approximately 0.7500 mT/mm. In fact, if we look at the value of the objective function in (2), namely

$$\int_0^T b_x^2(t) + b_y^2(t) dt \ ,$$

the 15 slice penalty results have an objective value of 0.1874 SAR units, whereas the generic RF pulse produced a value of 0.5923 SAR units. In addition, the 15 slice results generated the lowest objective value, 0.0385 SAR units.

Using the simulated gVERSE magnetization results, we produce two different graphs showing the transverse and longitudinal magnetization profiles. The desired magnetization distribution for a 90^0 RF pulse with 15 coordinate positions is shown in Figure 15, for further information about the desired profiles the reader may consult [8], [14]. The transverse magnetization profile illustrated in Figure 16 is very similar to what is desired in Figure 15. The M_x magnetization component is free of ripples and contains the requested step function. The M_y magnetization profile is included to illustrate its minimal presence. One should note that the lower axis in Figures 15 – 17 represents the magnetization vectors coordinate positions and from the results this corresponds to a distance of 60mm. The longitudinal magnetization profile in Figure 17 is also similar to what is implored, however, the M_z dip is slightly higher than desired. In both Figures 16 and 17 it is important to note that our resultant profiles have no ripples extending past the slice of interest, which is not the case for the results of [8], [9] and [19]. By virtually omitting ripples in our magnetization profiles we potentially reduce aliasing and other such factors that disrupt MR image resolution.

VI. Image Reconstruction

In Magnetic Resonance Imaging, the signal produced by the RF pulse is mathematically amplified, digitized, transformed, and then combined together with other signals to form a final image. There are several techniques that can be used to produce a final image, however, the core of the systematic procedure is the same for all methods. Principally, the signal or the raw data of measurements is directly related to the distribution of transverse magnetization in the object or specimen. There are different classes in which an image can be constructed using an RF pulse and as we are particularly interested in analyzing the performance of the gVERSE pulse, lower dimensional coverage is more suitable for our investigation. Thus, for our analysis we used 1D coverage.

A. gVERSE Simulation

An MRI simulation was implemented in Matlab to test the performance of the gVERSE pulse sequence where the pulse was set to collect data for 1D coverage. Using the Bloch equation we created an environment similar to that which is occurring in practical MRI. Thus, by providing the optimized gVERSE pulse sequence, the gradient and RF pulse values were supplied to a voxel of protons that would eventually form a final image. Specifically, the gVERSE values of $G(t_j)$, $b_x(t_j)$ and $b_y(t_j)$ for $j = 1, \ldots, N$ were read into the Bloch equation (1) for magnetization vectors at different $s_1, \ldots, s_n$ positions. Although we used a total of n coordinate

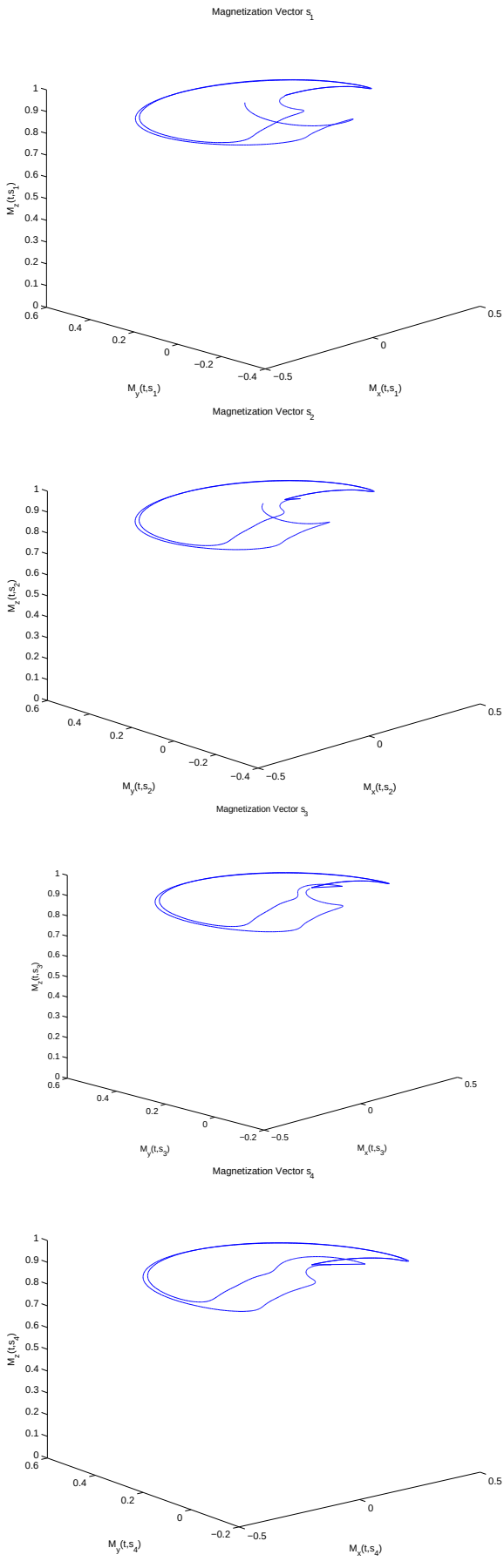

Fig. 11. From top to bottom, magnetization vectors corresponding to coordinate positions s_1, s_2, s_3 and s_4.

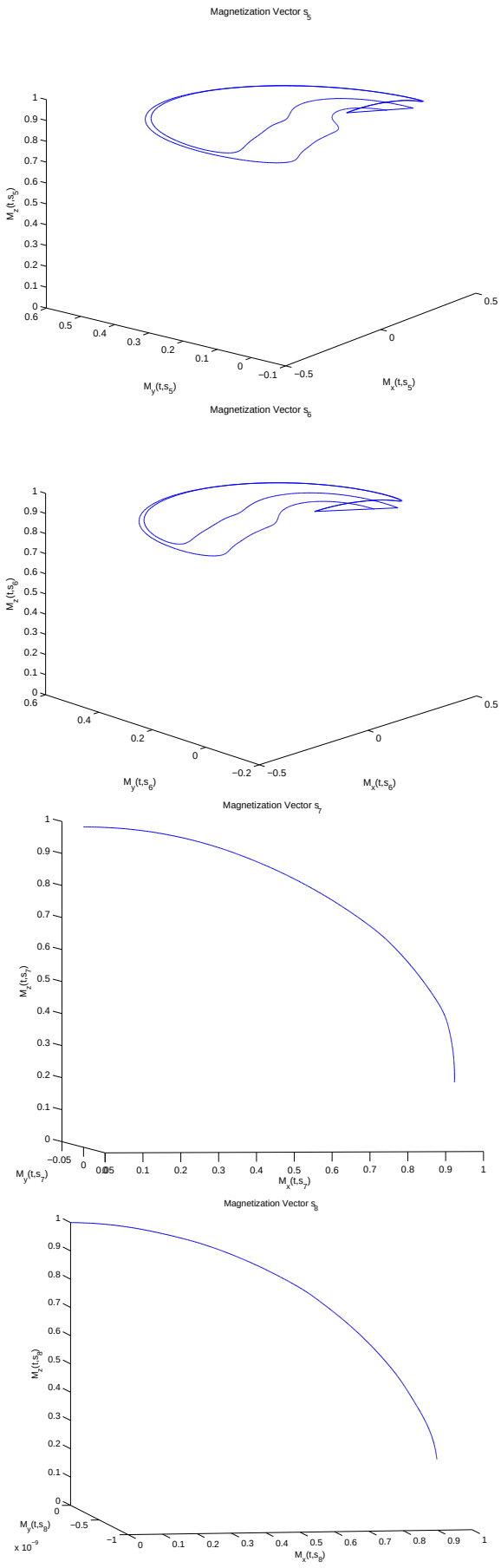

Fig. 12. From top to bottom, magnetization vectors corresponding to coordinate positions s_5, s_6, s_7 and s_8.

15 Slice Results

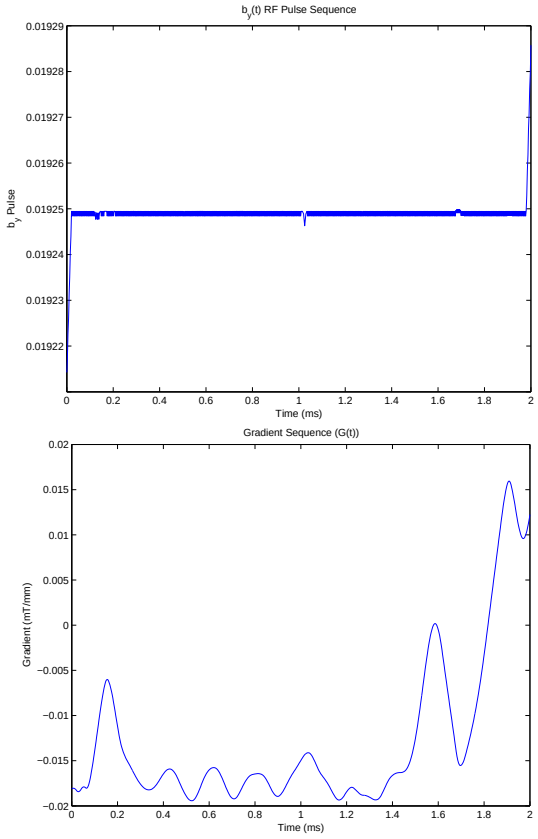

Fig. 13. External magnetization component $b_y(t)$ and gradient sequence $G(t)$ for the 15 slice results, $b_x(t)$ is zero.

15 Slice Penalty Results

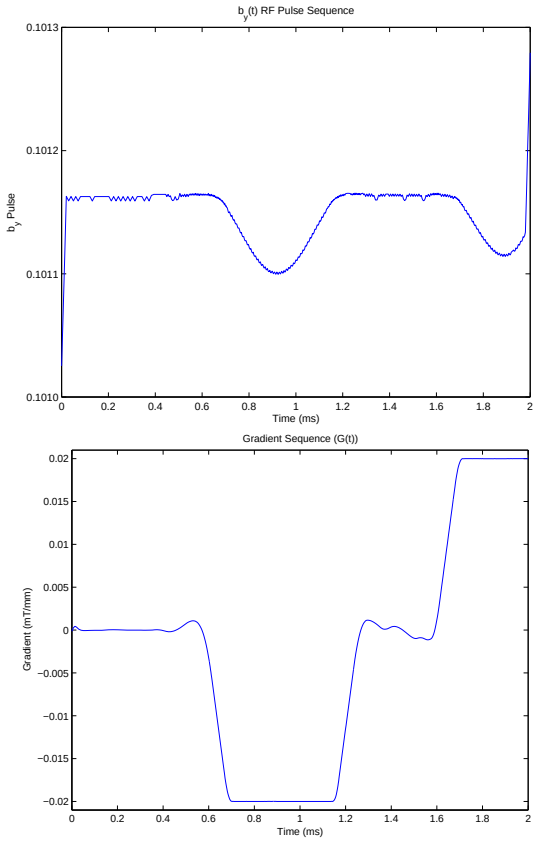

Fig. 14. External magnetization component $b_y(t)$ and gradient sequence $G(t)$ for the 15 slice penalty results, $b_x(t)$ is zero.

positions in the optimization of our model, the RF pulse and gradient sequence can be applied to $> n$ positions for imaging purposes. Thus, given $\overline{n} > n$ coordinate positions, N time discretizations, and an initial magnetization vector,

$$\overrightarrow{M}_0 = \begin{bmatrix} 0 \\ 0 \\ M_0 \end{bmatrix}, \tag{29}$$

the Bloch equation, namely

$$\begin{aligned} \frac{d\overrightarrow{M}(t_j, s_i)}{dt} &= \begin{bmatrix} M'_x(t_j, s_i) \\ M'_y(t_j, s_i) \\ M'_z(t_j, s_i) \end{bmatrix} \\ &= \begin{bmatrix} \gamma(-s_i G(t_j) M_y(t_j, s_i) + b_y(t_j) M_z(t_j, s_i)) \\ \gamma(s_i G(t_j) M_x(t_j, s_i) - b_x(t_j) M_z(t_j, s_i)) \\ \gamma(-b_y(t_j) M_x(t_j, s_i) + b_x(t_j) M_y(t_j, s_i)) \end{bmatrix}, \end{aligned} \tag{30}$$

was numerically integrated for each s_i value and $j = 1, \ldots, N$. The VESRE pulse sequence, $G(t_j), b_x(t_j)$ and $b_y(t_j)$, was then inserted into the integral of

$$\overrightarrow{M}(t, s_i) = \int_{t_1}^{t_N} \frac{d\overrightarrow{M}(\widehat{t}, s_i)}{dt}\, dt, \tag{31}$$

for $i = 1, \ldots, \overline{n}$ and where $\widehat{t} = [t_1, t_2, \ldots, t_N]^T$. The values for the magnetization vectors were then converted into a signal by simulating the amplification and digitization used in MRI. For a complete description of how (31) was integrated and amplified, one can refer to [18]. At this step we would be able to investigate the signal produced by our simulation and examine its properties. As mentioned in the preceding section, a signal with distinctive peaks and minimal noise would produce a high-quality final image. Also, by changing the value of M_0 in the initial magnetization vector, $\overrightarrow{M}_0$, we essentially replicate how an MRI processor would interpret different tissues or matter.

As there was relatively no difference with regards to simulation results using either of the gVERSE cases, the 15 slice penalty results were used. Using the gVERSE gradient and RF pulse sequence, many MRI simulations were conducted over various tissues. For the purposes of this paper we will show one of the results, for more simulation results the reader can see [18]. Using cerebrospinal fluid, the most significant results were tested by placing the tissue on an angle, as shown in Figure 18. As the signal generated by the pulse has a direct relationship with that of the tissues spin density, each tissues spin density value was substituted into M_0 at its respective position. Thus, a spin density value of 1.0 for cerebrospinal fluid was used when performing the MRI imaging simulation described earlier. Also note, the gVERSE pulse was designed to tip only the magnetization vectors in S_{in} into the transverse plane. Thus, the coordinate positions $s_i \in S_{\text{in}}$ would produce

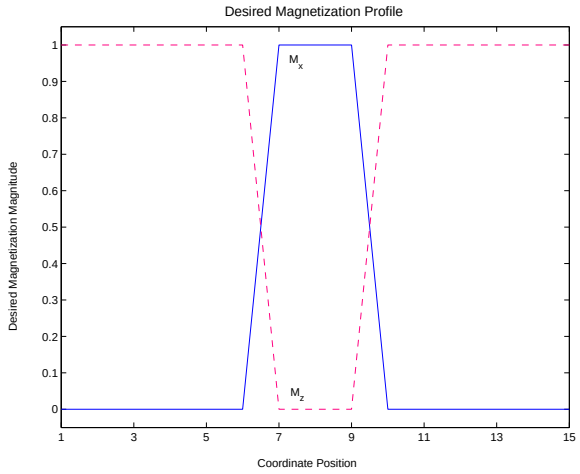

Fig. 15. Desired M_x and M_z distribution profiles for a 90^0 pulse.

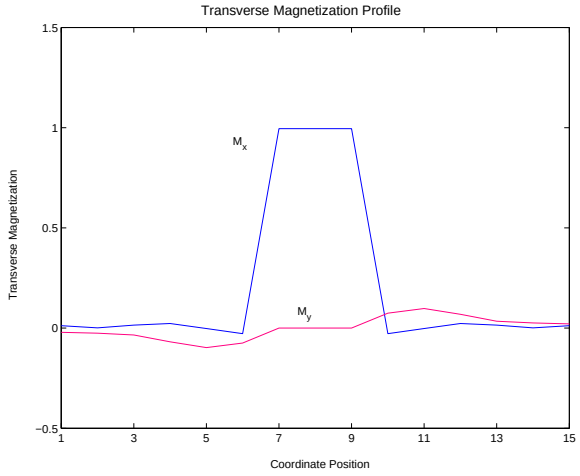

Fig. 16. Transverse magnetization components highlighting M_x and M_y magnitudes.

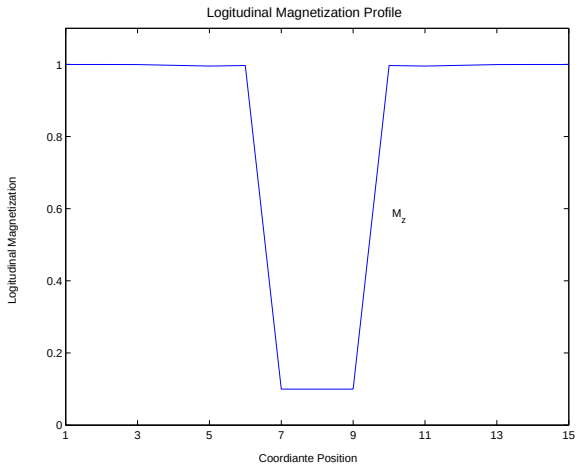

Fig. 17. Longitudinal M_z magnetization component magnitude.

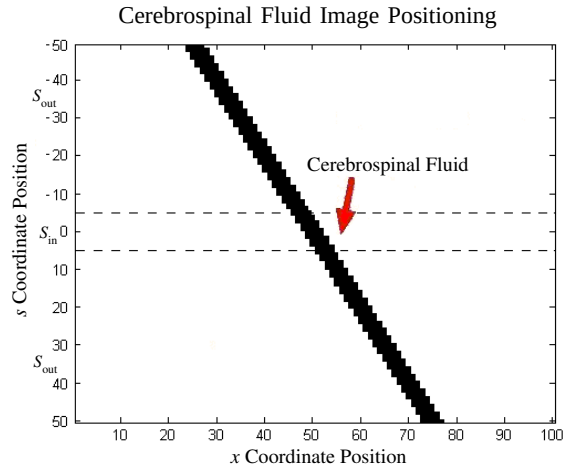

Fig. 18. The angular position of cerebrospinal fluid to be imaged by our MRI simulation.

a peak in the signal when the gVERSE pulse reaches the cerebrospinal fluid for these $s_i \in S_{\text{in}}$ voxels. As detailed in the preceding Sections, voxels $s_i \in S_{\text{in}}$ are located at the center coordinate positions, approximately -5 to 5 in Figure 18. Figure 19 represents the signal generated after the gVERSE RF pulse and gradient waveform was used to stimulate particular voxels within the cerebrospinal fluid into the transverse plane. As it is shown in Figure 19, the large central peak in the signal represents when the gVERSE pulse reaches the voxels in S_{in} of the fluid. The peak in the center of the figure is very distinctive and although noise was not integrated into the simulation, the signal produced a strong step function. Figure 20 represents the signal produced when a generic Sinc RF pulse and gradient waveform, described in Section IV, was used. In comparing Figure 19 to Figure 20, one can see that the signal produced by the gVERSE pulse has a more distinctive central peak and a much clearer division with regards to what is tissue and what is not. The base of the signal in Figure 19 is also more representative of when the voxels in S_{in} reach the fluid, which is not the case for the Sinc pulse. In addition, the objective

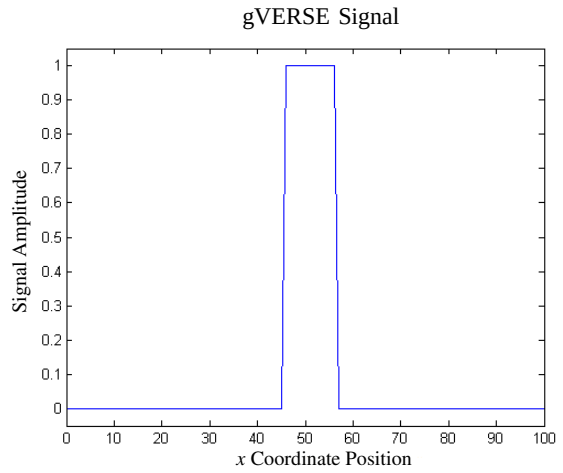

Fig. 19. The signal produced by the gVERSE pulse MRI simulation over the diagonal cerebrospinal fluid.

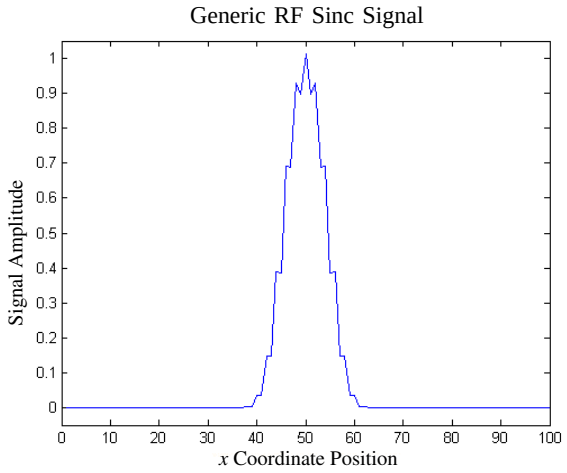

Fig. 20. The signal produced when a generic Sinc RF pulse and gradient sequence is applied to the diagonal cerebrospinal fluid.

value, which defines the strength of the RF pulse necessary to produce such a signal, was 0.1874 SAR units for the gVERSE pulse, substantially lower than that of the conventional pulse, which had an objective value of 0.5923 SAR units.

VII. Conclusions and Future Work

We designed the gVERSE model to reduce the SAR of RF pulses by maintaining a constant RF pulse strength ($\overrightarrow{B}_{\text{rf}}$ value) and generating high quality MR signals. It was shown that the gVERSE results produced strong MR signals with clear divisions of the location of the tissue being imaged. For this reason various MRI studies utilizing gVERSE pulses could be developed in the near future.

The observations noted in the Results Section deserve some additional reasoning and explanation. To begin, the reader should understand that the symmetry displayed between coordinate position vectors in each of the result cases was precisely designed in (11) of the gVERSE model. However, the precession illustrated by the magnetization vectors was not directly part of the gVERSE design, it was a consequence of the Bloch constraint (3). Nonetheless, the precession shown in our results validated our design since it occurs within the nucleus of atoms in vivo. Furthermore, investigating the precession of the magnetization vectors in the 15 slice results, it was shown that they had a much tighter radial orbit than the 15 slice penalty results. This was due to the fact that the penalty parameters allowed the feasible range of the constraints on these variables to be larger. With respect to precession, the 15 slice results were the most realistic. However, penalty variables in the 15 slice penalty results allowed the span of the magnetization vectors in S_{in} to be fairly large, which is probably what occurs in practice. In addition, investigating only the coordinate positions in S_{in} one should note that the penalty variables relaxed the constraints of the 15 slice penalty results, which did not induce the wave-like motion found in the vectors of the 15 slice results. One could conclude that in order to have improved transverse tipping and increase the length of magnetization vectors in S_{in}, larger ε_2 values are necessary, however, whether or not such a large precessional value is a realistic approximation would then become a factor.

The aim of the gVERSE pulse was to minimize SAR by maintaining a constant RF pulse ($b_x(t)$ and $b_y(t)$ values), which was established in both of the results. Although the values of $b_x(t)$ were identical for both cases, $b_y(t)$ values increased as the distance between the slices in S_{in} became larger. This was expected since an increase in the distance between $\overline{s}$ and $\underline{s}$ would require additional energy to tip the voxels into the transverse plane, yielding an increase in the strength of the RF pulse, or larger $b_y(t)$ value. The $b_y(t)$ values for the penalty results were the greatest and were not as constant as the other case. This was again due to the penalty variables and parameters, however, the nonlinear portions of the $b_y(t)$ graph only had small differences with respect to the other values; and they were lower. Also, when comparing the gVERSE pulse to conventional pulses the gVERSE objective value was lower for all cases, and hence, did not require as much energy to tip the magnetization vectors into the transverse plane. Finally, the most surprising part of the gVERSE pulse results is the gradient waveform. Since we optimized for the RF pulse in our model, this process returned the gradient waveform that would allow such a pulse to occur. In other words, in order to use the $b_x(t)$ and $b_y(t)$ pulse design, the accompanying gradient waveform, mainly derived from the Bloch constraint, would have to be imposed to acquire a useable signal. With regards to practical MR gradient waveforms, the 15 slice penalty results produced the simplest and most reasonable gradient vales to implicate, particularly due to its large linear portions. However, if necessary, regardless of the difficulty, either gradient could be implemented. Finally, both results had similar features in the sense that they each started off fairly negative and then ended up quite positive. This is a very interesting consequence of the gVERSE pulse, as shown in Section II and IV, conventional gradient sequences usually have the opposite characteristics. In terms of our MRI simulation, good signal results were produced for such unique gradient waveforms, which would justify further research with gVERSE pulses. In fact, Sections V and VI demonstrated that the gVERSE RF pulse and gradient sequence were viable and could be applied to practical MRI.

Future Work

The gVERSE pulse proved to have encouraging MRI results and performed to be better than anticipated with respect to useable MR imaging signals. However, there are still areas left for investigation and various elements of the gVERSE model can be improved. A few of the issues that should be taken into account for future developments are:

- Specializing the model to the rotating structure of the equations;
- Apply the gVERSE model to more than 50 slices;
- Add spin-lattice and spin-spin proton interactions to the gVERSE formulation;
- Apply alternative optimization software to the problem;
- Include gradient distortions to the gVERSE model.

The issues are listed in sequential order, starting with what we believe is the most important item to be addressed. As most are self explanatory, adding rotation into the equations was one of the factors that deemed to be important after the results were examined. By integrating the rotating frame of reference into our equations we eliminated the y-axis. It is possible that this was a source of singularities when optimizing and therefore caused $\mathbb{SOCS}$ to increase the size of its working array, occasionally creating memory problems. Although the memory problem was solved, further investigation is warranted to intelligently integrate rotation into our model.

ACKNOWLEDGMENT

This research was supported by NSERC Discovery grants, the CRC program, and MITACS.

REFERENCES

[1] D.P. Bertsekas. *Nonlinear Programming*. Athena Scientific, Belmont, Massachusetts, 1995.

[2] J.T. Betts. Issues in the Direct Transcription of Optimal Control Problems to Sparse Nonlinear Programs. *Control Applications of Optimization*, 115: 3-17, 1994.

[3] J.T. Betts. A Sparse Nonlinear Optimization Algorithm. *Journal of Optimization Theory and Applications*, 82: 519-541, 1994.

[4] J.T. Betts. *Practical Methods for Optimal Control Using Nonlinear Programming*. Society for Industrial and Applied Mathematics, Philadelphia, 2001.

[5] J.T. Betts and W.P. Huffman. Manual: Release 6.2 M and CT-TECH-01-014. The Boeing Company, PO Box 3707, Seattle, WA 98124-2207, 2001.

[6] S.C. Bushong. *Magnetic Resonance Imaging: Physical and Biological Principles*. Mosby, Toronto, 2nd edition, 1996.

[7] M.M. Connors and D. Teichroew. *Optimal Control of Dynamic Operations Research Models*. International Textbook Company, Pennsylvania, 1997.

[8] S.M. Conolly, D. G. Nishimura and A. Macovski. Optimal Control Solutoins to the Magnetic Resonace Selelctive Excitation Problem. *IEEE Transacitons on Medical Imaging*, MI-5: 106-115, 1986.

[9] S.M. Conolly, G. Glover, D.G. Nishimura and A. Macovski. Variable-Rate Selective Excitation. *Journal of Magnetic Resonance*, 78: 440-458, 1988.

[10] L. Cooper. *Applied Nonlinear Programming: for Engineers and Scientists*. Aloray Inc., Englewood, New Jersey, 1974.

[11] T.S. Curry, J.E. Dowdey and R.C. Murry. *Christensen's Physics of Diagnostic Radiology*. Lippincott Williams and Wilkins, New York, 4th edition, 1990.

[12] E. de Klerk, C. Roos, and T. Terlaky. *Nonlinear Optimization* (WI3 031). Delft University of Technology, 2003.

[13] Z. Liang and P. Lauterbur. *Principles of Magnetic Resonace Imaging*. Biomedical Engineering. Piscatawa, NJ: IEEE, 2000.

[14] E.M. Haacke, R.W. Brown, M.R. Thompson, and R. Venkatesan. *Magnetic Resonance Imaging: Physical Principles and Sequence Design*. John Wiley and Sons, Toronto, 1999.

[15] Z.P. Liang and P.C. Lauterbur. *Principles of Magnetic Resonance Imaging: A Signal Processing Perspective*. IEEE Press, New York, New York, 2001.

[16] D.G. Nishimura. *Principles of Magnetic Resonance Imaging*. Department of Electrical Engineering, Stanford University, 1996.

[17] J. Shen. Delayed-Focus Pulses Obtimized Using Simulated Annealing. *Journal of Magnetic Resonance*, 149: 234-238, 2001.

[18] S.J. Stoyan. *Variable Rate Selective Excitation RF Pulse in MRI*, Department of Mathematics, McMaster University, 2004.

[19] J.L. Ulloa, M. Guarini and P. Irarrazaval. Chebyshev Series for Designing RF Pulses Employing an Optimal Control Approach. *IEEE Transacitons on Medical Imaging*, 23: 1445-1452, 2004.

[20] X.L. Wu, P. Xu and R. Freeman. Delayed-Focus Pulses for Magnetic Resonace Imaging: An Evolutionary Approach. *Magnetic Resonance Medical*, 20: 165-170, 1991.